Coarse-Grained Simulations of the Membrane-Active Antimicrobial Peptide Maculatin 1.1

Peter J. Bond, Daniel L. Parton, James F. Clark, and Mark S. P. Sansom
Structural Bioinformatics and Computational Biochemistry Unit, Oxford Centre for Integrative Systems Biology, Department of Biochemistry, University of Oxford, Oxford, United Kingdom

ABSTRACT   Maculatin 1.1 (M1.1) is a membrane-active antimicrobial peptide (AMP) from an Australian tree frog that forms a kinked amphipathic α-helix in the presence of a lipid bilayer or bilayer-mimetic environment. To help elucidate its mechanism of membrane-lytic activity, we performed a total of $\sim$8 μs of coarse-grained molecular dynamics (CG-MD) simulations of M1.1 in the presence of zwitterionic phospholipid membranes. Several systems were simulated in which the peptide/lipid ratio was varied. At a low peptide/lipid ratio, M1.1 adopted a kinked, membrane-interfacial location, consistent with experiment. At higher peptide/lipid ratios, we observed spontaneous, cooperative membrane insertion of M1.1 peptide aggregates. The minimum size for formation of a transmembrane (TM) aggregate was just four peptides. The absence of a simple and well-defined central channel, along with the exclusion of lipid headgroups from the aggregates, suggests that a pore-like model is an unlikely explanation for the mechanism of membrane lysis by M1.1. We also performed an extended 1.25 μs simulation of the permeabilization of a complete liposome by multiple peptides. Consistent with the simpler bilayer simulations, formation of monomeric interfacial peptides and TM peptide clusters was observed. In contrast, major structural changes were observed in the vesicle membrane, implicating induced membrane curvature in the mechanism of active antimicrobial peptide lysis. This contrasted with the behavior of the nonpore-forming model peptide WALP23, which inserted into the vesicle to form extended clusters of TM α-helices with relatively little perturbation of bilayer properties.

INTRODUCTION

Antimicrobial peptides (AMPs), or host defense peptides, are short, amphipathic, cationic membrane proteins ($\sim$10–50 residues) secreted by many tissues in a variety of organisms. Over 880 such peptides have been characterized (1), ranging from human defensins to insect cercopins. AMPs have considerable therapeutic potential because they exhibit broad-spectrum antimicrobial activity and form part of the host's innate immune response. They can kill both Gram-positive and Gram-negative bacteria, as well as mycobacteria, fungi, and even coated viruses and transformed or cancerous cells (2). They are of interest because they present a possible solution to the increasing problem of bacterial resistance to antibiotics (3). This is because they do not bind to specific membrane protein receptors, as revealed by the fact that their activity is independent of amino acid chirality (4). Instead, they are thought to disrupt the lipid component of cell membranes. The cationic nature of AMPs results in a selectivity toward anionic bacterial cell membranes. Upon binding, they penetrate the cell membrane and induce lysis. However, their precise biophysical mode of action is not well defined, and may well vary from peptide to peptide (1).

The dorsal skin secretions of Australian tree frogs are especially rich in AMPs (2,5), which form part of the defense system of the animal and include the well-studied peptides citropin, aurein, and maculatin (2,4). These amphibian peptides adopt an α-helical conformation at the membrane surface, and upon interaction with the membrane they lead to its disruption. Several general mechanisms have been proposed to explain the action of AMPs (4). The simplest of these are the barrel-stave, toroidal pore, and carpet mechanisms. In both the barrel-stave and toroidal pore models (6), peptides aggregate at the membrane surface and subsequently insert to form a transmembrane (TM) ion-permeable pore. In the barrel-stave mechanism, the lipid headgroups remain located along the membrane surface (i.e., the local bilayer structure is preserved), with the pore surface lined solely by peptide helices. In the toroidal pore mechanism, peptides cause a local reorganization of the membrane leaflets, which curve so that the pore is lined by both peptide side chains and lipid headgroups. In contrast, in the carpet mechanism the peptides assemble with their axes parallel to the membrane, forming a carpet-like monolayer on the bilayer surface. This is suggested to lead subsequently to bilayer disruption in a detergent-like manner.

Maculatin 1.1 (M1.1) is a well studied but incompletely understood AMP. M1.1 is a wide-spectrum antimicrobial peptide from *Litoria genimaculata,* with the following sequence: GLFGV[5]LAKVA[10]AHVVP[15]AIAEH[20]F-NH$_2$ (see Fig. 1). Its structure has been resolved by NMR in both the nonaqueous solvent trifluoroethanol (TFE) and detergent (dodecylphosphocholine (DPC)) micelles (7). The peptide
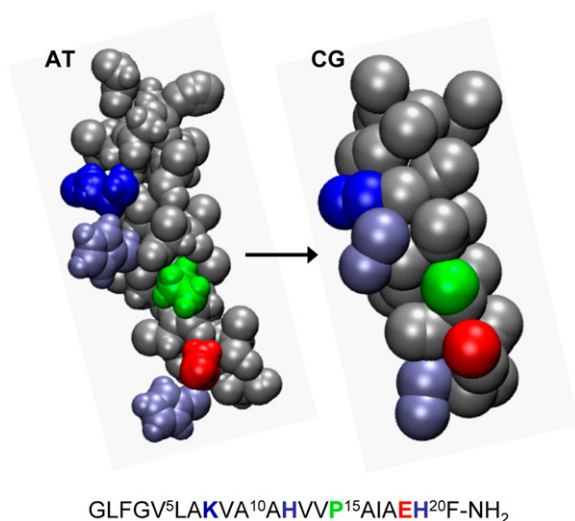

FIGURE 1 Structures of CG and AT structures of M1.1 in space-filling format. Red, E19 side chain; silver, backbone and hydrophobic side chains; dark blue, K8 side chain; light blue, H12 and H20 side chains; and green, P15.

adopts a similar conformation in both of these environments, namely, an amphipathic α-helix of length $\sim$30 Å, with a central kink in the vicinity of the central proline (P15) residue. The NMR structure of P15A M1.1, whose antibiotic activity is markedly reduced relative to the wild-type sequence, reveals a well defined helix lacking the central kink (7). The proline-induced kink (8,9) may be important in providing a well defined amphipathic surface for the peptide to interact with the membrane interface (10), and/or enabling partial penetration of the peptide into the bilayer, facilitating subsequent complete insertion (11).

Of interest, a number of experimental biophysical studies suggest that maculatin may exhibit different lytic mechanisms depending on the model membrane systems used. Thus, ^{31}P solid-state NMR spectroscopy data were interpreted as suggesting that the membranes of live Gram-positive bacteria are lysed by M1.1 via formation of micelle-like structures (7). Similarly, solid-state NMR studies combined with specific protein and lipid labeling showed that M1.1 was located in the interfacial region of dimyristoyl-phosphatidylcholine (DMPC) bilayers, and also that the long axis of the α-helix was at an angle of $\sim$50° to the bilayer normal, again suggesting a carpet, i.e., detergent-like, mechanism of membrane lysis (12). Electron microscopy revealed that M1.1 severely disintegrates cells of *Staphylococcus aureus*, suggesting that lysis in live cells may be due to an extreme case of the toroidal pore mechanism (4). On the other hand, studies in model phospholipid vesicles suggest a pore-forming mechanism (13). Attenuated total reflectance-Fourier transform infrared (ATR-FTIR) spectroscopy revealed that the angle of the helix axis of maculatin in membranes composed of dimyristoyl-phosphatidylglycerol (DMPG), and to a lesser extent DMPC, is $\sim$35° relative to the bilayer normal

(13). Moreover, solid-state NMR and oriented CD measurements in DMPC bilayers suggest a similar angle, albeit dependent on the lipid/protein ratio (11), thus suggesting a TM pore-forming model for insertion. Most recently, a novel method involving observation of leakage of two differently sized fluorescent molecules from giant unilamellar vesicles (GUVs) was developed (10). Upon addition of M1.1 peptides to GUVs, differential quenching of the two fluorescent probes was observed, suggesting that pores were formed by M1.1 through which only the smaller probe could pass. Significantly, the structure and integrity of the GUVs were preserved upon pore formation. Intriguingly, similar lytic behavior was observed in palmitoleoyl-phosphatidylcholine (POPC) and mixed POPC/palmitoleoyl-phosphatidylglycerol (POPG) vesicles, in contrast to that observed for DMPC versus DMPG bilayers (13). Thus, it remains unclear whether a carpet-like or pore-like (or both) model better describes the action of maculatin on membranes.

Atomistic molecular dynamics (MD) simulations provide a means to study in molecular detail the interactions of membrane peptides and proteins with lipid bilayers (14–18) or other lipid phases (19–22), and may be applied to more complex membrane-related processes, such as membrane protein folding (23), or vesicle fusion (24). Recently, an extended atomistic MD simulation study revealed the interaction of 2–4 molecules of magainin (an AMP related to maculatin) with a dipalmitoyl-phosphatidylcholine (DPPC) membrane (25). Spontaneous formation of nanometer-sized, toroidally shaped pores in the bilayer was observed.

In general, however, the time- and length scales accessible to all-atom (AT)-MD simulations are too short to observe spontaneous changes in complex protein/lipid systems that are directly comparable to both experimental measurements and biological phenomena. Coarse-grained (CG)-MD simulations, in which small groups of atoms are treated as single particles, provide a promising alternative (26–34) and have proved useful in enabling us to model the dynamics of lipid bilayers (26,27,35) and the interactions between lipid bilayers and membrane proteins (36–40). We have adapted one such model that has been applied extensively to lipids and membranes (26) for application to proteins. In this model, instead of representing each atom in a protein, water, or lipid molecule, particles corresponding to $\sim$4 atoms are used and are parameterized to capture the hydrophobicity/hydrophilicity, charge, and H-bonding properties of their constituent atoms. This method has been successfully applied to a number of membrane proteins and peptides (38–42).

Here we exploit the extended timescales available with coarse-grained molecular dynamics (CG-MD) to explore the interactions of M1.1 with zwitterionic phospholipid membranes (Table 1). The process of coarse-graining, illustrated in Fig. 1, results in preservation of the overall shape and surface exposure of the M1.1 peptide in the CG model compared to the starting atomistic structure, while it also reproduces the physicochemical properties of the component residues.

TABLE 1   Summary of simulations

Simulation name	System components	Peptide/lipid ratio	Box size (Å^3)	Number of simulations	Simulation time (ns)
1mac-sa	1 M1.1, 256 DPPC (random*), 3200 waters	1:256	$100 \times 100 \times 100$	9	200 or 300
16mac-bil	16 M1.1, 256 DPPC (bilayer*), ~5500 CG waters	1:16	$90 \times 90 \times 160$	5	200
16mac-bil-1μs	16 M1.1, 256 DPPC (bilayer*), ~5500 CG waters	1:16	$90 \times 90 \times 160$	3	1000
100mac-ves	100 M1.1, 877 POPC (vesicle*), ~55,000 CG waters	1:9	$210 \times 210 \times 210$	1	1250
100WALP-ves	100 WALP23, 877 POPC (vesicle*), ~55,000 CG waters	1.9	$210 \times 210 \times 210$	1	1250
Control-ves	877 POPC (vesicle*), ~60,000 CG waters	—	$210 \times 210 \times 210$	1	400

*Three classes of simulations were performed: self-assembly (sa) simulations in which the lipid molecules were initially placed at random within the simulation box, bilayer (bil) simulations in which the lipids were initially in a (planar) lipid bilayer, and vesicle (ves) simulations in which the lipids were in a vesicle.

In the current study we use CG-MD simulations to explore the mechanism of interaction of M1.1 with zwitterionic (DPPC) lipid bilayers, and we compare it with a synthetic peptide (WALP23) that does not exhibit antimicrobial activity (43,44). By varying the numbers of M1.1 and lipid molecules present in the simulations, we are able to demonstrate spontaneous adsorption and insertion of M1.1 peptide complexes leading to local bilayer disruption via formation of dynamic transbilayer aggregates of peptide molecules. Thus these simulations provide a direct insight into the mechanism of interaction of AMPs with liposomes, and are suggestive of the nature of the effect of AMPs on biological membranes.

MATERIALS AND METHODS

System setup

The structure of M1.1 used as the basis of all of these simulations was determined by solution-state NMR in a trifluoroethanol/water mixture and in dodecylphosphocholine micelles (7). This structure was converted to a CG model as described in Bond et al. (41) (Fig. 1). The CG model peptide was composed of a chain of backbone particles with attached side-chain particles. For all peptide simulations, the distance between backbone particles was restrained to mimic secondary structure H-bonds in the atomistic structure (38), using a harmonic distance restraint with an equilibrium length of 6 Å and a force constant of 10 kJ mol^{-1} Å^{-2}. Note that because proline lacks a hydrogen on the imide group, no H-bond restraint was present between Pro15 and Ala11, and their backbone particles were respectively treated as CG types ''Na'' and ''Nd'', rather than ''N0'' as described previously (38).

For the single-helix bilayer self-assembly simulations (1mac-sa; Table 1), the CG model of the M1.1 peptide was placed in the center of a box of dimensions $100 \times 100 \times 100$ Å^3. The system was subsequently combined with 256 randomly positioned CG DPPC lipid molecules, before solvation with ~3200 CG water particles. The system was then energy-minimized using <500 steps of the steepest-descent method to relax any steric conflicts between protein, lipid, and solvent. Multiple production simulations (using varying random seeds for initial velocities) were performed for 200–300 ns (Table 1).

For the multiple-helix bilayer simulations (16mac-bil), 16 M1.1 peptides were randomly added on either side of a preequilibrated CG 256-molecule DPPC bilayer in a box of dimensions $90 \times 90 \times 160$ Å^3, before solvation with ~5500 CG water particles. The system was then energy-minimized using <500 steps of the steepest-descent method to relax any steric conflicts between protein, lipid, and solvent. Multiple production simulations (using varying random seeds for initial velocities) were performed for 200–1000 ns.

For the control vesicle (Control-ves) simulation, coordinates were downloaded from the Marrink CG web site (http://md.chem.rug.nl/~marrink/ MARTINI/Coordinates.html) of an 877-palmitoleoyl-phosphatidylethanolamine (POPE) vesicle containing ~60,000 CG water particles in a box of dimensions $210 \times 210 \times 210$ Å^3. The lipids were converted from POPE to POPC by appropriate modification of their headgroup particles, and the solvated POPC vesicle system was energy-minimized using <500 steps of the steepest-descent method to relax any steric conflicts between lipid and solvent. A production simulation of 400 ns was then performed.

For the multiple-helix vesicle simulation (100mac-ves), 100 M1.1 peptides were randomly added outside the outer leaflet of the ''control'' 877-POPC vesicle. Subsequently, the system was solvated with ~55,000 CG water particles in a box of dimensions $210 \times 210 \times 210$ Å^3. The system was then energy-minimized using <500 steps of the steepest-descent method to relax any steric conflicts between protein, lipid, and solvent. A production simulation of 1.25 μs was then performed.

A multiple-helix vesicle simulation (100WALP-ves) was also run using the nonpore-forming peptide WALP23 (43,44) (see Table 1). The peptide was modeled as an idealized α-helix and then converted to a CG model. The 100WALP-ves system was prepared in the same way as the 100mac-ves system, and a 1.25 μs production simulation was then performed.

Simulation protocol

Simulations were performed using GROMACS (www.gromacs.org) (45,46). CG simulations were performed as described in Bond and Sansom (38), with CG parameters for lipid and water molecules as in Marrink et al. (26), and for amino acids as in Bond and Sansom (38), with minor modifications to bond and angle potentials as described in Bond et al. (47).

Lennard-Jones interactions were shifted to zero between 9 Å and 12 Å, and electrostatics were shifted to zero between 0 Å to 12 Å, with a relative dielectric constant of 20. The nonbonded neighbor list was updated every 10 steps. All simulations were performed at constant temperature, pressure, and number of particles. The temperatures of the protein, lipid, and solvent were each coupled separately using the Berendsen algorithm (48) at 323 K, with a coupling constant $\tau_T = 10$ ps. The system pressure was anisotropically coupled using the Berendsen algorithm at 1 bar with a coupling constant $\tau_P = 10$ ps and a compressibility of 1×10^{-5} bar^{-1}. The timestep for integration was 40 fs. Simulations were performed on Linux workstations and a 30-node dual-core Linux cluster. Analyses were performed using GROMACS tools and locally written code. Visualization used visual molecular dynamics (VMD) (49) and RasMol (50).

RESULTS AND DISCUSSION

Simulations performed

Three classes of simulations were performed, as summarized in Table 1. In self-assembly (1mac-sa; Fig. 2 A) simulations a single M1.1 molecule was surrounded by lipid molecules that
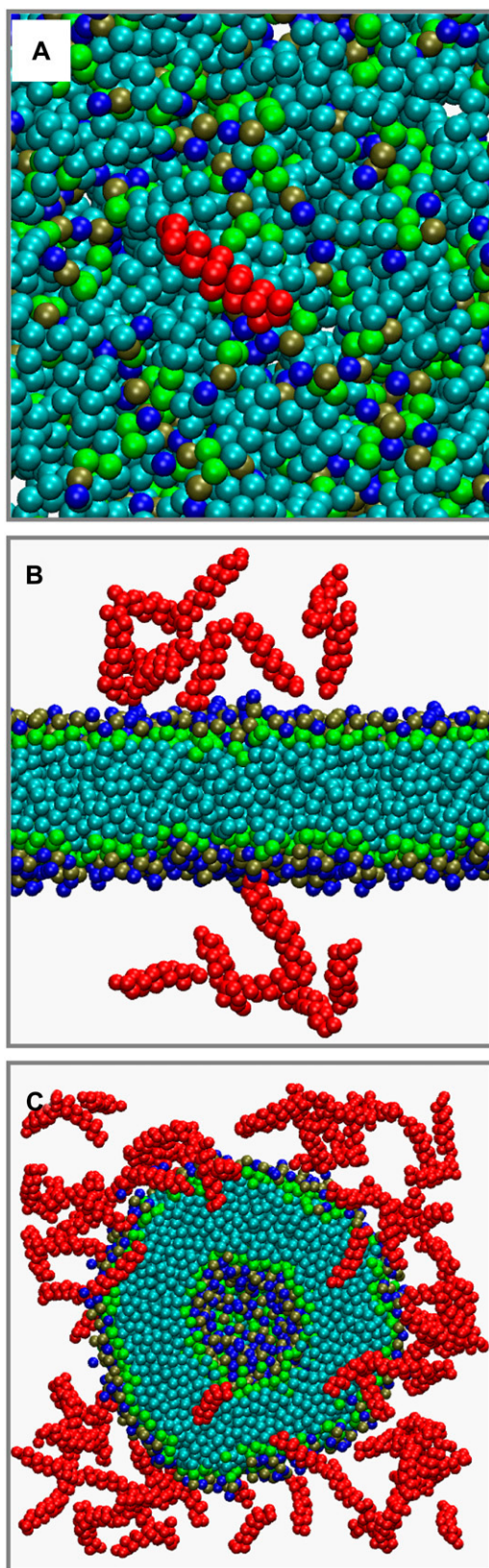
FIGURE 2 Starting snapshots for each simulation system in space-filling format. In each snapshot, red = backbone particles of M1.1 peptides; and cyan, green, tan, and dark blue = lipid tail, glycerol backbone, phosphate,

were initially placed at random locations/orientations within the simulation box to discover the preferred location of monomeric M1.1 relative to a (self-assembled) bilayer. In the bilayer (16mac-bil and 16mac-bil-1μs; Fig. 2 B) simulations the lipids were initially in a (planar) lipid bilayer, with 16 M1.1 molecules in the aqueous phase. Finally, in the vesicle (100mac-ves; Fig. 2 C) simulation a small (diameter ~200 Å) vesicle was surrounded by 100 M1.1 molecules, initially in the (external) aqueous phase. Thus the bilayer and vesicle simulations allow us to model the interactions of multiple M1.1 molecules with a preformed bilayer, mimicking the interactions of M1.1 with membranes in vitro. Note that these simulations also explored peptide/lipid ratios ranging from 1:256 (1mac-sa) to ~1:9 (100mac-ves).

Single helix simulations

Self-assembly simulations (1mac-sa) were performed beginning from a system containing randomly-positioned lipids and water plus a single M1.1 peptide, at a peptide/lipid ratio of 1:256 (Fig. 2 A). In each simulation a lipid bilayer spontaneously formed, proceeding via a stalk-intermediate between the bilayer and its periodic image, as described previously for both CG (26,38) and atomistic (51) simulations. The mean time for bilayer formation was 60 ± 60 ns. In three of the nine simulations, upon bilayer formation the M1.1 peptide was observed to be at an interfacial location with an in-plane orientation (Fig. 3, A and B). In the other six simulations, the peptide adopted a TM orientation upon bilayer formation, but subsequently (within 10 ns) switched to an interfacial position. In none of the simulations was the peptide observed to either flip back to a TM orientation or to dissociate from the bilayer once it had adopted an interfacial orientation. Thus, the CG self-assembly simulations suggest that the preferred orientation for monomeric, bilayer-associated M1.1 is approximately perpendicular to the bilayer normal, at the interface between the hydrophobic acyl tails and the polar lipid headgroups.

While the M1.1 peptide remained stably anchored at the membrane interface in all the 1mac-sa simulations, some variations in the helix conformation and the depth of penetration into the bilayer were observed. From the distributions of tilt angles of the M1.1 peptide with respect to the bilayer normal, and of helix kink angles around the P15 residue (Fig. S1 of the Supplementary Material, Data S1), the M1.1 helix was most frequently observed at an angle of ~75–90° to the bilayer normal, with a small kink of ~15–30° in the center of the helix (Fig. 3 A). A degree of variation in the helix kinking about the P15 hinge (Fig. S1 A, Data S1) was observed (as permitted by the parameterization of the restraints around the

and choline particles, respectively. (A) Single-helix, DPPC bilayer self-assembly simulations (1mac-sa). (B) Multiple-helix, DPPC preformed bilayer simulations (16mac-bil). (C) Multiple-helix, POPC vesicle simulation (100mac-ves).
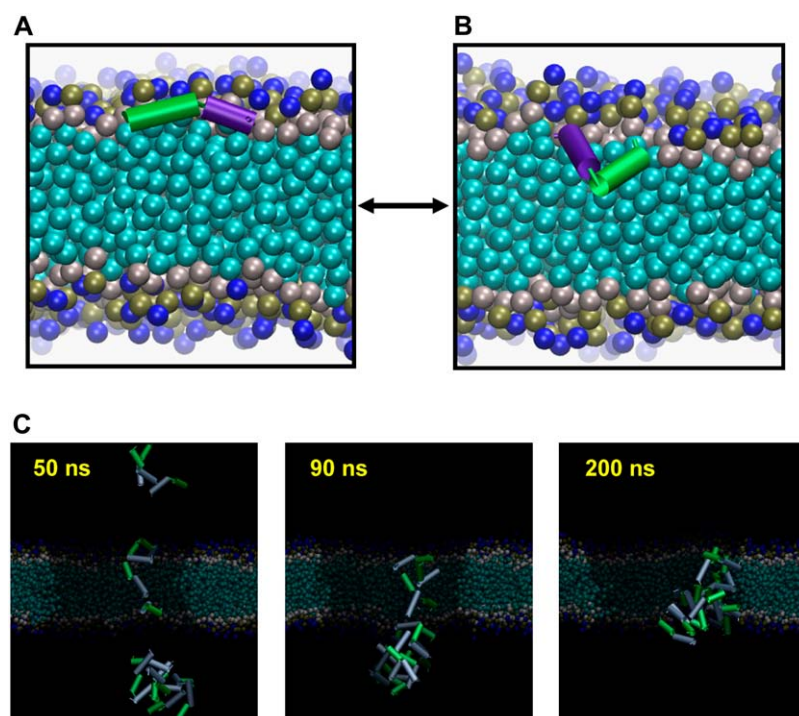
FIGURE 3 (*A* and *B*) Representative snapshots from the 1mac-bil simulations, after bilayer self-assembly. In *A*, the approximately straight M1.1 peptide is shown anchored to the membrane interfacial region. In *B*, the peptide has kinked at P15 residue and is ''dipping'' into the hydrophobic core of the bilayer. (*C*) Snapshots of a representative peptide integration pathway (see text for details), with time frames indicated, from one of the 200 ns duration 16mac-bil simulations. In each snapshot, the N- and C-terminal halves of the M1.1 peptide backbone are shown in green and sky blue cartoon formats, respectively, centered around the kink-inducing P15. The DPPC lipid particles are shown in space-filling format, colored as follows: cyan, green, tan, and dark blue = lipid tail, glycerol backbone, phosphate, and choline particles, respectively.

proline), with kink angles of up to ~150° observed. As illustrated in Fig. 3 *B*, this more pronounced kinking process often occurred alongside a greater degree of penetration of the peptide into the bilayer core. The N-terminal half of M1.1 seems to facilitate this process of semiinsertion, possibly because the lysine residue (K8) is able to ''snorkel'' toward the interfacial region. It therefore seems likely that this kinking process may facilitate TM insertion of M1.1 peptides, as seen under conditions of increased peptide/lipid ratios (see below). This is therefore consistent with previous experimental studies indicating that the α-helical peptide may lie around the headgroup region but may also partially insert into the membrane core as a result of the kink-inducing proline (11,12).

Multiple helix bilayer simulations

Having established that the preferred location of a single M1.1 helix is at the bilayer/water interface, we next performed simulations with multiple peptides (16mac-bil) at a higher peptide/lipid ratio (1:16) starting from a preformed bilayer with M1.1 helices in the surrounding aqueous phase (Fig. 2 *B*). These conditions were designed to model the multiple-peptide complexes required for propagation of antimicrobial membrane lysis via the carpet or pore mechanisms. They also mirror the conditions used for a range of structural, biophysical, and activity measurements of M1.1 and other AMPs (4). Five simulations of duration 200 ns (16mac-bil) were run to enable observation of the initial aggregation behavior. Three of these were extended to 1 μs (16mac-bil-1μs; Table 1) to follow the long-timescale behavior of the M1.1 aggregates within the membrane.

In each of these simulations, the M1.1 peptides were observed to rapidly (within 10 ns) aggregate together, reducing the solvent exposure of their hydrophobic helices while simultaneously adsorbing to the bilayer surface. Subsequently, membrane insertion was observed over a timescale approximately an order of magnitude slower.

The peptide aggregation process may be quantified by examining the sizes of the peptide clusters over time (Fig. 4 *A*). A peptide is defined as being part of a cluster if any of its constituent particles are <6 Å from the particles of another peptide (or cluster of peptides). A rapid (~10–20 ns) initial aggregation phase was observed, during which several small clusters formed and then fused to form at least one large cluster of ≥12 peptides. Subsequently, over the following ~100 ns, in all but one of the five 16mac-bil simulations, all peptides fused to form a complete cluster of 16 M1.1 peptides. In the remaining simulation, a cluster varying between 14 and 16 peptides was observed (Fig. 4 *A*). During the process of M1.1 aggregation, adsorption of the peptide clusters to the bilayer surface was also observed. Concurrently, these clusters inserted into the bilayer core, as revealed by the simultaneous, gradual increase in the number of peptides in contact (<6 Å) with both lipid headgroup and acyl tail particles (data not shown), with insertion times ranging from ~100 to 200 ns. A slightly asymmetric peptide distribution with respect to bilayer leaflets was normally observed upon insertion, so that by 200 ns, on average ~15 vs. ~11 peptides were in contact with either opposing leaflet.

Multiple pathways for ''clustering and insertion'' seemed to be followed. The minimum cluster size required for initial TM insertion was just 4 M1.1 molecules (Fig. 3 *C*, 50 ns).
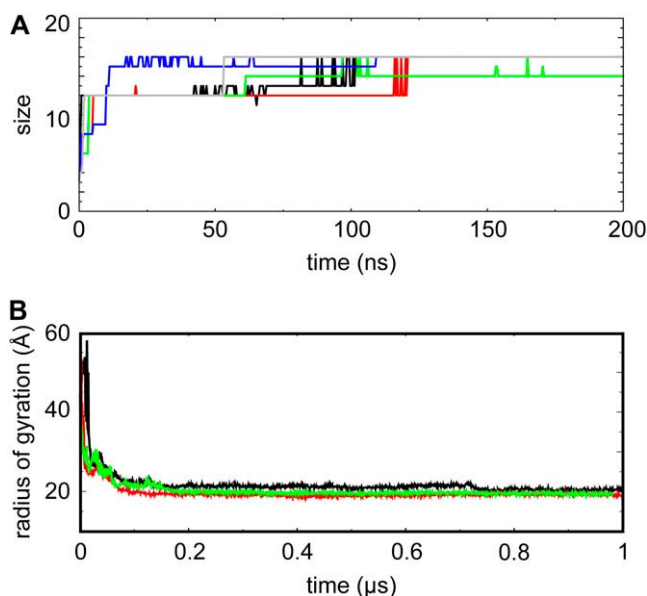
FIGURE 4   Behavior of peptide aggregates during 16mac-bil simulations. (*A*) The size of M1.1 peptide clusters during the 200 ns duration 16mac-bil simulations I (*black*), II (*red*), III (*green*), IV (*blue*), and V (*gray*). A peptide is defined as part of a cluster if any of its constituent particles are <6 Å from the particles of another peptide (or cluster of peptides). (*B*) Radius of gyration for all peptide backbone particles during the 16mac-bil-1μs simulations I (*black*), II (*red*), and III (*green*).

(This has also been seen in both atomistic and CG simulations of the related peptide magainin H2 (25,52).) Of these small TM clusters, only one peptide typically traversed the bilayer, while the remaining peptides were located in an in-plane, interfacial orientation. These ''peripheral'' peptides were nevertheless flexible, resulting in kinking around P15 and partial insertion into the membrane core (Fig. 3 *C*, 90 ns), as observed for the single peptide 1mac-sa simulations (see above). These minimal TM aggregates are reminiscent of results from a recent atomistic MD study of magainin, where small, spontaneously formed toroidal pores consisted of a single peptide in the bilayer center along with a few parallel peptides at the edge of the pore (25). Over more extended timescales, it was observed that the small TM aggregate attracted larger, extramembranous peptide clusters, subsequently nucleating fusion and bilayer insertion of the entire complex (Fig. 3 *C*). Alternative scenarios are also observed in which several variously sized clusters adsorb to the surface of one or both bilayer leaflets, again with their component helices in a primarily parallel orientation. Subsequently, the complexes fuse while also converting to TM complexes, but they often proceed through intermediates involving just a single TM peptide. In some cases large peptide complexes were observed to form outside of the membrane and then adsorb onto the surface. These subsequently traversed the bilayer core, approximately maintaining the aggregate structure achieved out of the membrane, with minor changes in the orientation of individual helices, e.g., at the interfacial region

where several helices adopt an approximately perpendicular orientation relative to the bilayer normal.

The membrane-inserted M1.1 aggregates had compact structures that for the most part excluded lipid molecules, and in particular, lipids did not curve or deform significantly to enable headgroups to penetrate the aggregates. The peptide clusters had rather ill-defined structures, as illustrated by analysis of the longer-timescale (i.e., 16mac-bil-1μs) simulations. Consistent with the membrane insertion of these complexes, the mean distribution of tilt angles of the M1.1 peptides (Fig. S2, Data S1) revealed a large increase in the number of helices arranged in an approximately parallel orientation with respect to the bilayer normal, in comparison with the single helix 1mac-sa simulations (Fig. S1, Data S1). Thus, an increased peptide/lipid ratio favors helix kinking and hence penetration of interfacially located peptides into the bilayer. This may not only aid insertion of individual peptides, but perhaps more importantly may enable interaction with already-inserted TM helices, thus stabilizing their localization in the bilayer core, especially during the initial stages of aggregate insertion (see, e.g., Fig. 3 *C*). Upon insertion, the precise internal arrangement of M1.1 peptides with respect to one another within a particular aggregate remained stable for timescales of at most ~50 ns, with frequent periods of ~200 ns during which a particular cluster was dynamically changing (as indicated by the root mean-squared deviation (RMSD) of a peptide cluster, calculated with respect to its respective structure 40 ns previously; Fig. S3, Data S1). Nevertheless, the clusters remained in a membrane-inserted state, diffusing only within the bilayer plane, and maintained a globally constant shape, as indicated by the preservation of the maximum cluster size of 16 peptides (data not shown) throughout the simulations.

The radius of gyration (Rg) of a M1.1 peptide cluster over the course of the simulation describes its size evolution (Fig. 4 *B*). This confirmed that the primary changes in aggregate dimensions occurred within the first ~200 ns, whereas the final Rg was ~2 nm for each simulation. Thus, the TM aggregates are irregular, fluctuating structures, which nevertheless remain complexed together. The presence of peripheral, kinked peptides at the bilayer interfacial region that ''dip into'' the core enable the central TM peptides to remain stably inserted.

Vesicle simulations

Three simulations of POPC vesicles of diameter ~200 Å were performed: one in the absence of M1.1 (i.e., a control simulation, control-ves), a second in which the vesicle was initially surrounded by 100 randomly-placed M1.1 helices (100mac-ves; Fig. 2 *C*), and a third in which the vesicle was initially surrounded by 100 randomly placed WALP23 helices (100WALP-ves). The 100mac-ves simulation was designed to model the interaction of AMPs with biological membranes that exhibit bilayer curvature and in which only

one face of the bilayer is exposed to peptide. The conditions also mirror the higher lipid:protein ratios utilized during a number of in vitro studies, including recent fluorescent-probe leakage measurements made upon addition of M1.1 to POPC vesicles (10). The 100WALP-ves simulation was included as a control, using a peptide that is suggested to self-associate within membranes but does not form pores (53).

The 100mac-ves simulation allowed the observation of spontaneous adsorption and insertion of M1.1 peptide complexes into the vesicle membrane, the description of which has been broadly separated into three main stages: 1), an initial, fast (~0–100 ns) process of peptide/peptide aggregation; 2), an intermediate stage (~100–300 ns) of peptide clustering and lipid adsorption/insertion; and 3), a slower relaxation stage over the remainder of the simulation (Fig. 5).

The initial phase (0–100 ns). During the first ~50–100 ns, peptides rapidly aggregate, as seen from the distribution of clusters of peptides over time (Fig. 6 A). It may thus be observed that in the first ~100 ns, ~15 small clusters of ~5–15 peptides each are formed (for further cluster analysis, see Fig. S4, Data S1). Many of these clusters also adsorb to the vesicle surface, as shown by the increase in number of peptide molecules in contact (<6 Å) with the heads and tails of outer leaflet lipid molecules (Fig. 7 A). Within ~100 ns, ~70 peptides have come into contact with both the outer leaflet headgroups and also, interestingly, tails. This appears to be because the clusters of M1.1 peptides form patches on the surface of the vesicle, and their hydrophobic α-helical regions penetrate into the outer leaflet acyl tail particles, forcing lipid headgroups away from this region. Indeed, this cluster insertion process means that even a few particles of the inner leaflet tails are contacted by (~20) peptides over this short timescale (Fig. 7 A). Of the few peptides which are still monomeric after ~100 ns, these lie on the surface of the vesicle in an interfacial, in-plane orientation, with no evidence of TM insertion (Fig. 5 A). Thus, peptide aggregation may be necessary to form sufficiently large patches devoid of lipid headgroups, easing peptide access to the hydrophobic acyl tails.

The intermediate phase (100–300 ns). Over the next ~200 ns, there is a gradual, stepwise increase in the number of M1.1 peptides in contact with the outer leaflet tails and headgroups, as the remaining clusters in the aqueous phase adsorb to the vesicle (Fig. 7 A). Thus, by ~300 ns, there are ~85–90 contacts with both outer leaflet tails and headgroups. There are a total of ~90–95 peptide molecules in contact with all lipids (i.e., tails or headgroups), and this remains approximately constant for the remainder of the 1.25 μs simulation. At the same time, there is also an increase in the number of peptides in contact with the lipids of the *inner* leaflet as peptide clusters begin to penetrate into the interior of the vesicle (Fig. 7 A). Visual inspection reveals that these are made primarily by the peptide clusters already adsorbed to the outer vesicle surface at ~50–100 ns (Fig. 5). Of interest, between ~0–300 ns, there are several sudden stepwise
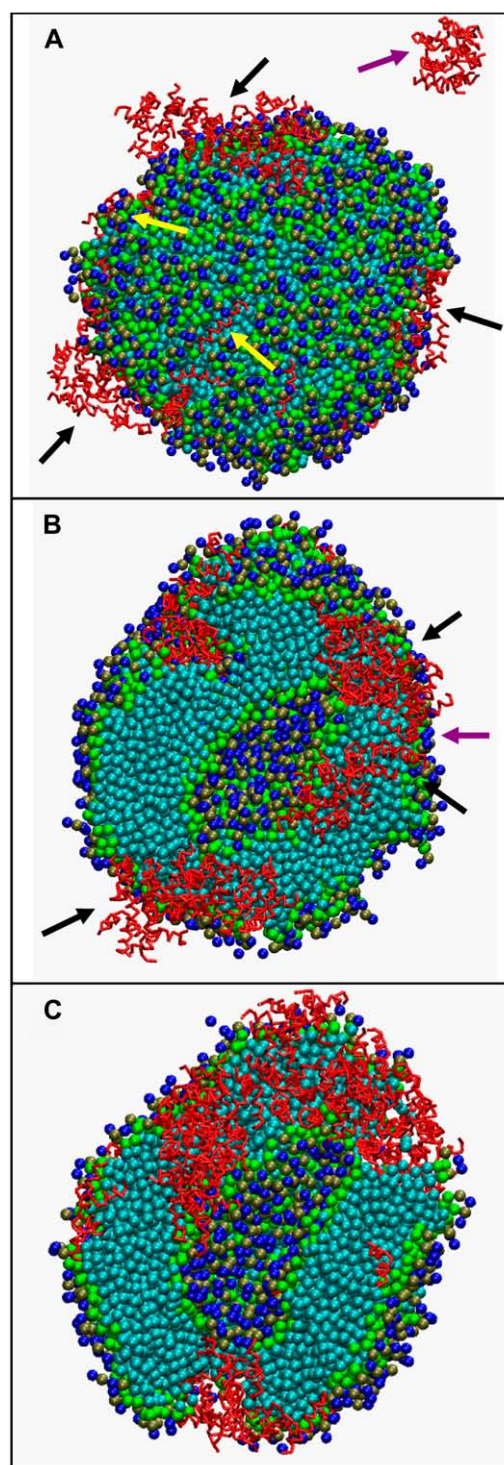

FIGURE 5 Snapshots from the 100mac-ves simulation at (*A*) 50 ns, (*B*) 300 ns, and (*C*) 1250 ns. *B* and *C* are "cut through" the vesicle to reveal its cross section. (*A*) A peptide cluster in solution (*purple arrow*), three peptide clusters adsorbed to the vesicle surface (*black arrows*), and groups of monomeric/dimeric peptides adsorbed to the surface (*yellow arrows*). (*B*) Three membrane-integrating peptide clusters (*black arrows*), two of which later fuse to form a larger peptide aggregate (purple arrow). (*C*) Two TM peptide clusters are evident. In each snapshot, the M1.1 peptide is shown in red backbone format. For the POPC lipids, cyan, green, tan, and dark blue = lipid tail, glycerol backbone, phosphate, and choline particles, respectively.
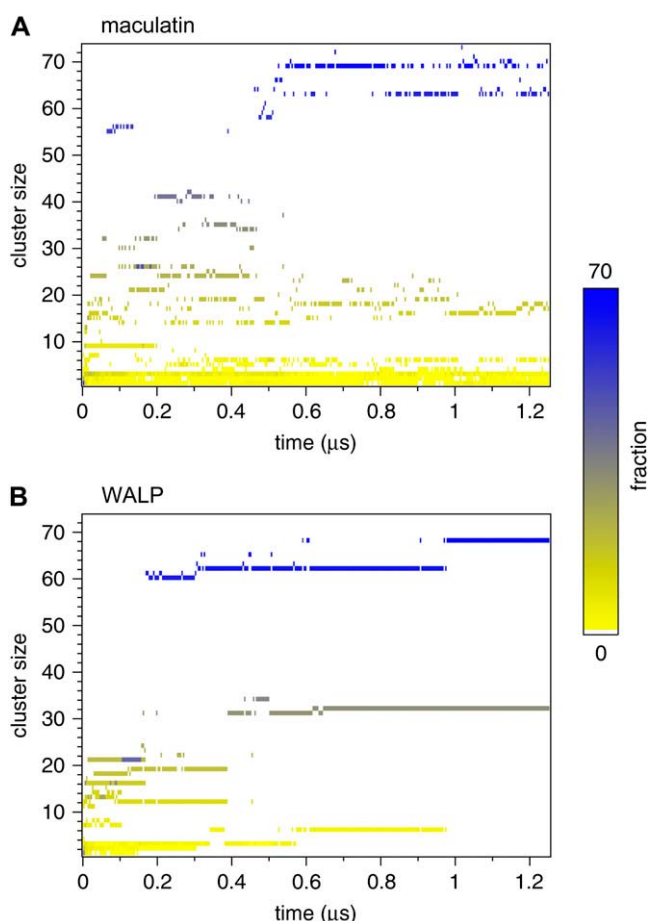
FIGURE 6   Distribution of cluster sizes for peptides in the (A) 100mac-ves and (B) 100WALP-ves simulations. A peptide is defined as part of a cluster if any of its constituent particles are <6 Å from the particles of another peptide (or cluster of peptides.) At any time, each cluster is colored to represent its size as a fraction of the total number of clusters present (yellow = 0%, blue = 100%).

jumps in inner leaflet tail contacts (Fig. 7 A). In each case, ~50 ns after each of these tail-contacting events, similar patterns are observed for peptides contacting the inner leaflet headgroups. By ~300 ns, there are ~45 M1.1 molecules in contact with the inner tails, and ~25 in contact with the inner headgroups. Moreover, visual inspection reveals that there are three component clusters making the majority of these contacts, of sizes ~15, ~25, and ~40 peptides (Fig. 5, *arrows*). Thus, on average, by this stage about half of the M1.1 peptides in a "penetrating" cluster are able to contact the inner leaflet tails, and only about half of those (i.e., about a quarter of each peptide cluster) are able to interact with the inner interfacial region. A range of orientations are observed for the peptide molecules that interact with the inner leaflet headgroups, as discussed further below.

By ~300 ns, all protein clusters are in contact with the vesicle, and no further changes occur in *total* protein-lipid contacts. Over this period there are also morphological changes in the vesicle as a whole. Thus, the Rg for the vesicle

lipids gradually increases from ~55 Å nm at 0 ns (as in the control-ves simulation) and plateaus at ~57 Å by ~300 ns. This does not change significantly over the remainder of the simulation (Fig. 8 A). Thus, protein adsorption/insertion apparently results in an increase in the mean size of the vesicle, as confirmed by the rapid reduction in the Rg of the protein *plus* lipid as a whole, which reduces rapidly from ~75 Å at 0 ns and levels off at ~62 Å by ~300 ns (Fig. 8 A).

Changes in the overall morphology of the vesicle may be quantified by the three time-averaged principal moments of inertia (MOIs): I_1, I_2, and I_3. The POPC control vesicle is approximately spherical, with a ratio of $I_1/I_2/I_3 \approx$ 1:1:1 throughout the control-ves simulation. In contrast, there is a gradual change over the first ~300 ns of the 100mac-ves simulation to a ratio for the vesicle lipids of $I_1/I_2/I_3 \approx$ 1.3:1.2:1 (Fig. S6, Data S1). Thus, the vesicle has become more ellipsoidal. This change is even more evident when the peptide is included in the calculation; the ratio is ~1.5:1.3:1, reflecting the overall asymmetric distribution of M1.1 molecules within the vesicle membrane. If one calculates the MOI for the lipids of the inner leaflet only, the ratio becomes $I_1/I_2/I_3 \approx$ 1.7:1.5:1 by ~300 ns (Fig. S7, Data S1). This occurs because of the smaller number of lipids in the inner leaflet and consequently increased lamellar curvature. Overall, it appears that the clustering, adsorption, and subsequent penetration of M1.1 peptides induces a significant degree of "stretching" of the vesicle along its principal axis.

The changes in vesicle shape are reflected at the molecular level by altered dynamics of the constituent lipids. The mean second-rank order parameter $P_2 = \langle 1/2 \ (3\cos^2\theta - 1) \rangle$ was calculated for each of the lipid bonds of the inner and outer leaflets (Fig. 9 A). Here, θ is defined as the angle between the bond of interest and a vector connecting the center of the bond to the center of mass of the vesicle (i.e., approximating the local membrane normal), with $P_2 = 1$ representing perfect normal alignment of a bond, $P_2 = -0.5$ representing perfect antialignment, and $P_2 = 0$ reflecting a random orientation. It should be noted that these values did not significantly change in the 100mac-ves simulation after ~300 ns. It is clear that for the control-ves simulation, the order parameters for the inner and outer lipids are largely similar along the chain, with random alignment of the choline-phosphate bond, an approximately semialigned orientation for the phosphate-glycerol bond, and then gradually decreasing order along the lipid tails, again attaining an almost random alignment at the ends of the acyl tails. Slightly more disorder is observed for the lipid tails of the inner leaflet. This overall pattern resembles a similar order parameter profile obtained for a CG vesicle containing DPPC lipids (54). Analyzing the 100mac-ves simulation, it seems that the lipids of the outer leaflet behave in a manner similar to that of the control vesicle, with only slightly reduced order for the phosphate-glycerol and glycerol-tail bonds. However, there is a striking reduction in the order parameters for the bonds connecting, in particular, the headgroup and glycerol backbone particles, along with
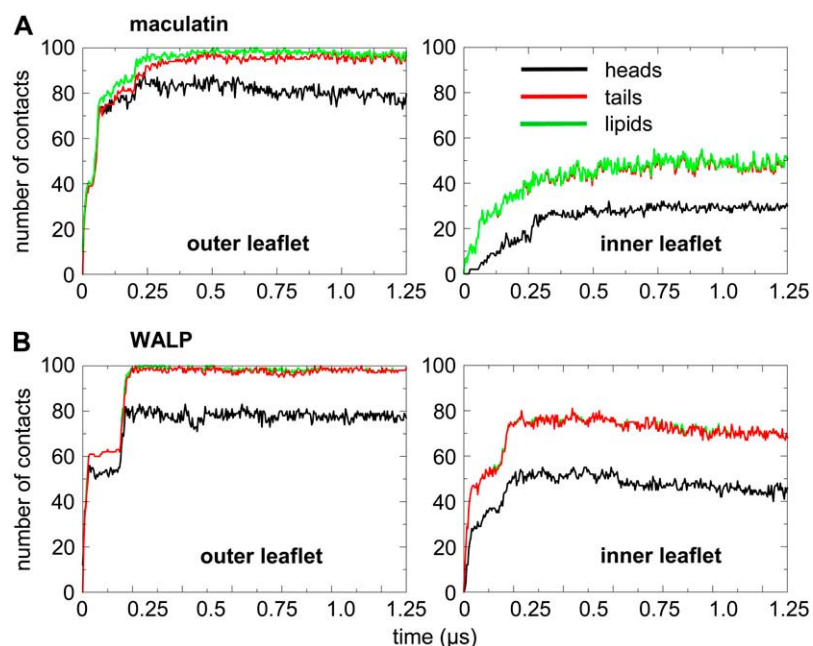
FIGURE 7 Number of peptide molecules in contact (<6 Å) with lipid during the (*A*) 100mac-ves and (*B*) 100WALP-ves simulations. Results are shown for interactions with total lipid (green), as well as the headgroups (black) and tails (red) of the outer (left-hand panels) and inner (right-hand panels) vesicle leaflets. Headgroups are defined as the choline, phosphate, and glycerol backbone groups. Tails are defined as all other remaining lipid particles.

the first few tail particles. Thus, the morphological changes in the vesicle that lead to ''stretching'' along the principal axis result primarily in a reduction in ordering of bonds of the inner leaflet lipids. Evidently, the high induced curvature of

FIGURE 8 Radius of gyration for lipid only (gray line) and for lipid and protein (black line) during the (*A*) 100mac-ves and (*B*) 100WALP-ves simulations.

the inner leaflet is compensated for by a disordering of individual lipids, easing the global changes in the shape of the vesicle as it is ''stretched''.

Significantly, at ~300 ns, when the vesicle shape has more or less stabilized, the largest M1.1 clusters that have penetrated the vesicle bilayer, allowing peptides to interact with the inner leaflet, are clearly located at the ''poles'' of the ellipsoidal vesicle. By definition, the bilayer curvature, and thus lateral membrane tension, is greatest at the poles of the now-ellipsoidal vesicle. Thus, the ''stretching'' of the vesicle and clustering of protein aggregates at either ''pole'' facilitates the gradual, stable insertion of M1.1 peptides into the inner leaflet. This is a consequence of the locally increased membrane tension, which results in membrane thinning around the penetrating clusters and a decrease in the structural order of lipids of the inner leaflet. Both effects appear to ease the transition of peptides into the bilayer core.

The final phase (300 ns onward). The vesicle shape does not change substantially over the remainder of the 1.25 μs simulation, although there are still some changes in peptide aggregation. At ~400 ns, the two large TM clusters composed of ~40 and ~25 peptides begin to fuse with one another (Fig. 6 *A*). Subsequently, for the remainder of the simulation, the average population of all clusters consists of the two main ''polar'' clusters of ~60–70 and ~15–20 peptides each (Fig. 5 *C*). Of these peptide aggregates, visual inspection reveals that, similar to the peptide/vesicle complex at 300 ns, about a third to a quarter of the individual peptides in each cluster interact directly with the inner leaflet headgroups. This final fusion event seems to accompany a slightly deeper penetration of peptide clusters, with a loss of ~5 outer leaflet headgroup contacts and a corresponding increase in inner leaflet tail contacts.
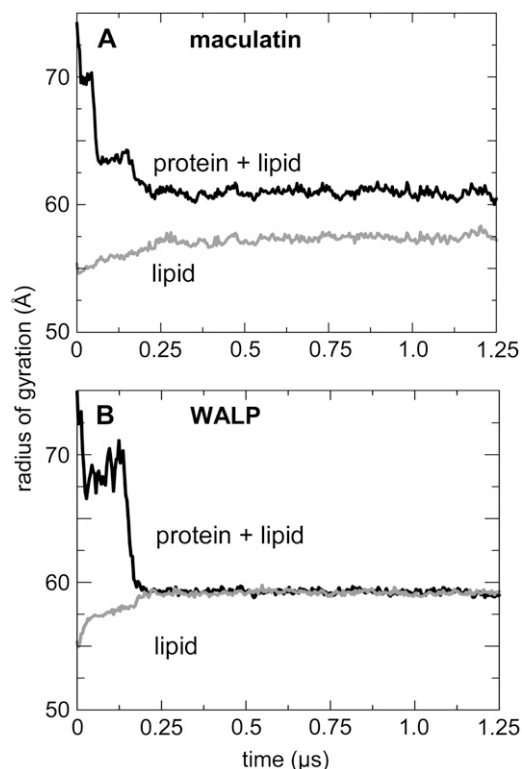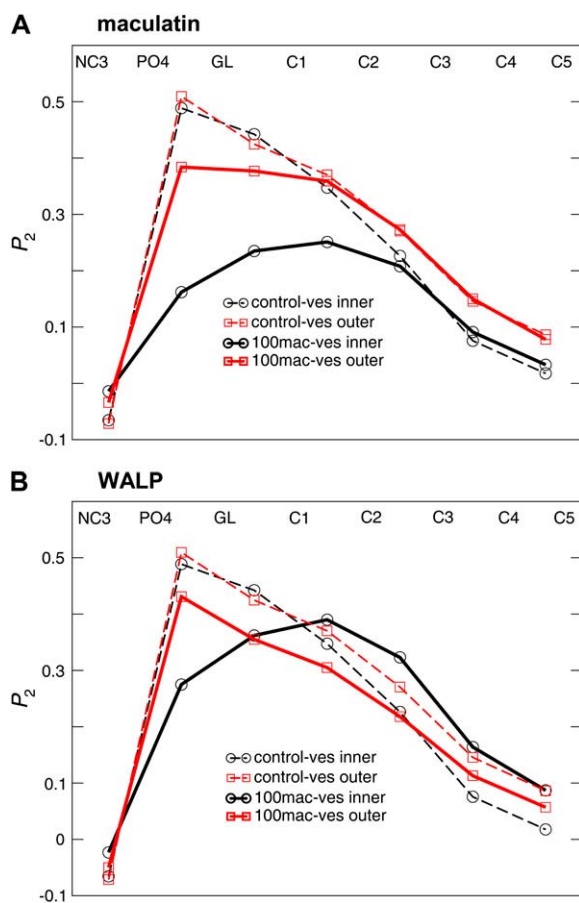
FIGURE 9 P_2 order parameters for lipid bonds of the inner (black) and outer (red) vesicle leaflets for the (A) 100mac-ves and (B) 100WALP-ves simulations. In each case the order parameters for the simulation in the presence of peptides (solid lines) are compared with those of the control-ves (dashed lines) simulation for a vesicle in the absence of peptides. Order parameters are approximately calculated with respect to the vesicle surface normal, as described in the text. Values are shown for consecutive bonds between the choline (NC3), phosphate (PO4), glycerol backbone (GL), and acyl tail (C1-C5) particles (as indicated by labels). The mean order parameters were calculated after discarding the initial 200–400 ns of each simulation.

Visual inspection suggests that the vesicle cavity remains "stretched" along the proteoliposome principal axis, particularly in the vicinity of the two peptide aggregates localized at the "poles" (Fig. 5). Thus, while already in contact with the inner leaflet at 300 ns, these aggregates continue to optimize their lipid-protein interactions over the course of the simulation, becoming more intimately associated with the headgroups (Fig. 5). This is partly a result of changes in peptide orientation/dynamics. The average tilt angle of the peptides with respect to the bilayer surface normal was estimated by calculating the angle between a vector fitted to the backbone particles of each helix and a vector connecting the center of each helix to the center of mass of the vesicle. As in previous simulations, a range of tilt angle distributions were observed, skewed toward an in-plane orientation. Although a

modal tilt angle of 75–90° was observed throughout the simulation (Fig. S8 A, Data S1), when all peptide clusters are adsorbed to the vesicle at the end of the simulation, the overall distribution is flatter, with an increase in the number of peptides tilted at an angle of <45° with respect to the bilayer normal.

Thus, with respect to a simple bilayer environment, as the simulation proceeds and M1.1 peptides become more incorporated into the vesicle membrane, a shift occurs from single-helix-like (cf., the 1mac-sa simulations, Fig. S1 B, Data S1) to multiple-peptide behavior (cf., the 16mac-bil simulations, Fig. S2 B, Data S1). Moreover, although the kink angle distribution changes little as the 100mac-ves simulation proceeds (Fig. S8 B, Data S1), the modal kink angle range is higher (30–45°) than for either of the bilayer systems (Figs. S1 A and S2 A, Data S1) for which the mode was 15–30°. Thus, a combination of the high peptide/lipid ratio along with the increased membrane curvature of the vesicle phase leads to a greater degree of peptide kinking, again aiding stable insertion of M1.1 peptides.

It is informative to compare the behavior of WALP23 (which does not form pores in membranes) with that of maculatin in the vesicle simulations. The clustering pattern for WALP23 is rather different from that of maculatin (Fig. 6), suggesting the formation of a small number of less-disperse clusters for WALP23. Differences in the structures of the clusters formed are reflected in their protein-lipid interactions. Thus, while both types of peptide insert rapidly into the vesicle, many more WALP23 helices form contacts with the inner leaflet lipids compared to maculatin (Fig. 7). This reflects the greater tendency of WALP23 to adopt a TM orientation, which is also indicated by the mean tilt angles with respect to the vesicle surface normal for the two species of peptide (data not shown). Similarly, the radii of gyration of the lipid alone and of the lipid plus protein have the same final values for WALP23, in contrast to the situation for maculatin (Fig. 8). This is again consistent with a more equal distribution of peptide residues across the vesicle bilayer for the nonpore-forming WALP23 compared to maculatin.

There is also a pronounced difference between the two types of peptide in terms of their effects on the lipid order parameters (Fig. 9). For M1.1 the effects on order parameters were relatively small (as discussed above) in the outer leaflet, with a distinct decrease in order in the inner leaflet. In contrast, the order of the inner leaflet lipid tails is actually increased in the presence of WALP23, and the decrease in order around the glycerol region is less pronounced. This is presumably a result of the WALP23 peptides adopting a TM orientation, thus being able to pack uniformly within the vesicle membrane and causing less vesicle distortion and lipid disruption compared to maculatin (Fig. 10). Indeed, estimates of MOIs (data not shown) indicate that WALP23 has significantly less of an effect on the "elongation" of the vesicle.

Overall, the groups of inserted M1.1 peptides in the vesicle simulation consist of compact, lipid-excluded aggregates,
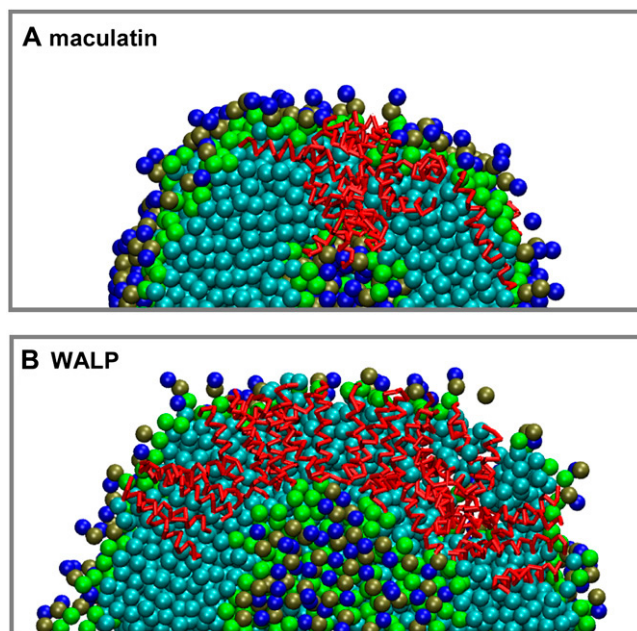
FIGURE 10 Representative snapshots of final peptide clusters for the (*A*) 100mac-ves and (*B*) 100WALP-ves simulations. In each snapshot, the peptide is shown in red backbone format, and the lipids in space-filling format with cyan, green, tan, and dark blue = lipid tail, glycerol backbone, phosphate, and choline particles, respectively.

lined on either vesicle leaflet at the bilayer interfacial region by many in-plane helices, some of which kink toward the membrane center to stabilize a few fully TM peptides, which nevertheless tilt to different degrees with respect to the local membrane normal. In contrast, the WALP23 peptides form more ordered TM helix bundles. Thus, even at the CG level there is a clear difference in the qualitative and quantitative behavior of pore-forming and nonpore-forming α-helical peptides.

CONCLUSIONS

These long-timescale CG-MD simulations have enabled us to explore the interactions of M1.1 with zwitterionic phospholipids over a range of peptide/lipid ratios and with various lipid configurations, including a large-scale and extended simulation of the permeabilization of a vesicle by multiple peptides. Single-helix self-assembly simulations demonstrated that the preferred position of monomeric M1.1 is at the membrane interface with an in-plane orientation. Nevertheless, the kinking dynamics of the helix around the central P15 residue were observed to favor the partial penetration of the peptide, particularly its N-terminal half, which contains a lysine that can ''snorkel'' toward the lipid headgroups upon semiinsertion.

The observed average location and kinking behavior of the monomeric M1.1 α-helix are consistent with experimental studies (11,12) and suggest that helix insertion may require

the interactions of multiple helices. It is difficult to obtain experimental evidence for the exact numbers of helices in *transient* peptide clusters. However, for alamethicin (albeit a rather different system), pores form with >12 helices (as reviewed in, e.g., Sansom (55)). It therefore does not seem unreasonable to suggest that large assemblies are formed by other AMPs. We therefore tested the ability for M1.1 to insert into preformed bilayers at a higher peptide/lipid ratio. These simulations revealed the cooperative membrane insertion of M1.1 peptide aggregates. Before the formation of larger clusters, the minimum size of an aggregate required for a TM orientation of one or more M1.1 helices was just four peptides, as previously observed for the toroidal magainin pores observed in both atomistic MD simulations (25). As predicted, the insertion of each aggregate, small or large, was stabilized by peripheral interfacial helices that kinked into the membrane core to support deeper TM helices. Similar structures have been seen in recent CG simulations of pores formed by the AMP magainin-H2 (52).

The arrangement of peptides within each membrane-inserted aggregate within the bilayer phase was dynamic and underwent significant fluctuations, but the approximate shape and size of each cluster was maintained over a microsecond. Importantly, the peptide aggregates exhibited compact structures, which for the most part excluded lipid molecules. Occasionally, a central, pore-like cavity could be identified within an aggregate, but this was only transient and did not exhibit water passage during the simulated timescales. It is probable that the CG level of representation, with four waters approximated by a single particle, may prevent the observation of such events. Thus, it may be beneficial to convert the M1.1 aggregate structures into an AT representation via a multiscale approach to investigate this possibility (31,56,57).

Indeed, there are a number of limitations to the CG approach. In particular, it cannot reproduce atomistic detail and so cannot fully capture the likely role of peptide-water-ion and lipid-water-ion interactions in membrane permeabilization/lysis. It will also be of interest to see how improved CG force fields (52,58) may refine our model of maculatin/bilayer interactions. However, in the longer term, the solution to the limitations of CG methods (such as the absence of a detailed treatment of water) may be to combine CG and AT models together in a multiscale approach (31,32,56,57). This would combine the ability of CG approaches to model large-scale self-assembly and membrane reorganization events with the ability of extended AT-MD simulations to refine initial structural models of peptide/lipid/water interactions (59). Indeed, it may even be necessary to extend such multiscale methods to include polarizable water models (60), given, e.g., discussions of electroporation as a possible mechanism of pore formation (61,62). Such multiscale simulations would also allow us to explore, e.g., detailed changes in peptide conformation upon peptide clustering.

However, at the present stage, in the absence of fully atomistic detail, our results indicate that the absence of a well-

defined and long-lasting central pore, and the exclusion of lipid headgroups from the aggregates make either the barrel-stave model or the toroidal pore model an unlikely explanation for the mechanism of membrane lysis by M1.1. This is very different from models of classical pore-forming peptides such as alamethicin (55), reflecting the different nature of their interactions with lipid bilayers.

These simulation results led us to ask how the interaction of M1.1 peptides with a liposome, which has direct relevance to experimental studies (4), might inform our understanding of the mechanism of lysis. An extended 1.25 μs simulation revealed the spontaneous adsorption and insertion of multiple M1.1 peptide complexes into a vesicle membrane. This proceeded via initial, rapid peptide-peptide aggregation accompanying adsorption of the peptides to the vesicle surface, followed by a slower (>100 ns) process of peptide cluster TM insertion. Monomeric peptides on the surface of the vesicle remained in an interfacial, in-plane orientation, with no evidence of TM insertion, thus resembling the single helix bilayer simulations. In contrast, clusters of peptides were sufficient to form large patches on the vesicle surface devoid of lipid headgroups, hence ''opening up'' the bilayer and easing access to the hydrophobic acyl tails. As the simulation proceeded, some of these clusters were able to penetrate further and fully integrate into the membrane over hundreds of nanoseconds, with about a third of each cluster becoming associated with the lipid headgroups of the inner leaflet. Again, this was aided by kinking around the central Pro residue of interfacial M1.1 peptides at the edge of each cluster, and the final aggregates resembled their counterparts in the multiple-peptide bilayer simulations.

An important difference between the bilayer and vesicle simulations was the morphological changes in the structure of the membrane. The process of TM integration of peptide clusters seemed to ''stretch'' the vesicle along one axis, resulting in a more ellipsoidal shape and hence an increased membrane tension as a result of induced curvature, particularly for the inner leaflet due to its greater lipid density compared to the outer leaflet. This was further evidenced by a reduction in order parameters for the bonds of the inner leaflet lipids. Accompanied by this was the TM insertion of two peptide clusters located at either end, or ''pole'', of the axis along which the vesicle was observed to be stretched. Thus, the ''stretching'' of the vesicle and reduction in inner leaflet lipid order eased peptide aggregate incorporation into the membrane, particularly at the resultant vesicle ''poles'' where the membrane tension due to curvature is highest and lipid order is lowest.

Critically, these morphological changes in the vesicle membrane were stable, and over a microsecond timescale the vesicle actually began to resemble two curved, stacked bilayers around the two main TM peptide aggregates in cross section (Fig. 6). Thus, the global membrane structure is clearly destabilized, and it is possible that over more extended timescales the vesicle could become ''torn'' near the aggregates where the bilayer curvature stress is still high, resulting in dramatic increases in bilayer permeability. This might be tested via a more CG approach, as in a recent study that showed that clustered model proteins adsorbed on lipid bilayer membranes could induce membrane curvature and vesicle formation (63). Thus, our observations suggest that M1.1 may in fact proceed via a modified, curvature-destabilizing carpet mechanism. Rather than serving as a necessarily ''detergent-like'' model for bilayer disruption at the surface, the M1.1 peptides appear to form stable, lipid-excluded complexes that modify membrane structure by changing the local spontaneous curvature (particularly of the inner leaflet), and may eventually bend it enough to cause local and/or global lysis of the proteoliposome. This is in contrast to the behavior of, e.g., TM helices as represented by the WALP23 peptide.

We note that the current simulations are limited to zwitterionic lipids. In the future, such studies will be extended to more complex lipid mixtures (including anionic lipids). To fully explain lipid selectivity, it may of course be necessary to employ multilevel simulations, i.e., combining CG and atomistic approaches. It will also be of interest to extend these simulations to establish the extent to which our observations may be generalized to a wider range of AMPs.

SUPPLEMENTARY MATERIAL

To view all of the supplemental files associated with this article, visit www.biophysj.org.

REFERENCES

1. Brogden, K. A. 2005. Antimicrobial peptides: pore formers or metabolic inhibitors in bacteria? *Nat. Rev. Microbiol.* 3:238–250.

2. Apponyi, M. A., T. L. Pukala, C. S. Brinkworth, V. M. Maselli, J. H. Bowie, M. J. Tyler, G. W. Booker, J. C. Wallace, J. A. Carver, F. Separovic, J. Doyle, and L. E. Llewellyn. 2004. Host-defence peptides of Australian anurans: structure, mechanism of action and evolutionary significance. *Peptides.* 25:1035–1054.

3. Lewis, K. 1994. Multidrug resistance pumps in bacteria: variations on a theme. *Trends Biochem. Sci.* 19:119–123.

4. Boland, M. P., and F. Separovic. 2006. Membrane interactions of antimicrobial peptides from Australian tree frogs. *Biochim. Biophys. Acta.* 1758:1178–1183.

5. Lazarus, L. H., and M. Attila. 1993. The toad, ugly and venomous, wears yet a precious jewel in his skin. *Prog. Neurobiol.* 41:473–507.

6. Oren, Z., and Y. Shai. 1998. Mode of action of linear amphipathic α-helical antimicrobial peptides. *Biopolymers.* 47:451–463.

7. Chia, B. C. S., J. A. Carver, T. D. Mulhern, and J. H. Bowie. 2000. Maculatin 1.1, an anti-microbial peptide from the Australian tree frog,

Litoria genimaculata—solution structure and biological activity. *Eur. J. Biochem.* 267:1894–1908.

8. Cordes, F. S., J. N. Bright, and M. S. P. Sansom. 2002. Proline-induced distortions of transmembrane helices. *J. Mol. Biol.* 323:951–960.

9. Bright, J. N., and M. S. P. Sansom. 2003. The flexing/twirling helix: exploring the flexibility about molecular hinges formed by proline and glycine motifs in transmembrane helices. *J. Phys. Chem. B.* 107:627–636.

10. Ambroggio, E. E., F. Separovic, J. H. Bowie, G. D. Fidelio, and L. A. Bagatolli. 2005. Direct visualization of membrane leakage induced by antibiotic peptides: maculatin, cercopin, and aurein. *Biophys. J.* 89:1874–1881.

11. Marcotte, I., K. L. Wegener, Y.-H. Lam, B. C. S. Chia, M. R. R. de Planque, J. H. Bowie, M. Auger, and F. Separovic. 2003. Interaction of antimicrobial peptides from Australian amphibians with lipid membranes. *Chem. Phys. Lipids.* 122:107–120.

12. Balla, M. S., J. H. Bowie, and F. Separovic. 2004. Solid-state NMR study of antimicrobial peptides from Australian frogs in phospholipid membranes. *Eur. Biophys. J.* 33:109–116.

13. Chia, B. C. S., J. Torres, M. A. Cooper, I. T. Arkin, and J. H. Bowie. 2002. The orientation of the antibiotic peptide maculatin 1.1 in DMPG and DMPC lipid bilayers. Support for a pore-forming mechanism. *FEBS Lett.* 512:47–51.

14. Forrest, L. R., and M. S. P. Sansom. 2000. Membrane simulations: bigger and better? *Curr. Opin. Struct. Biol.* 10:174–181.

15. Ash, W. L., M. R. Zlomislic, E. O. Oloo, and D. P. Tieleman. 2004. Computer simulations of membrane proteins. *Biochim. Biophys. Acta.* 1666:158–189.

16. Bond, P. J., and M. S. P. Sansom. 2004. The simulation approach to bacterial outer membrane proteins. *Mol. Membr. Biol.* 21:151–162.

17. Domene, C., P. J. Bond, S. S. Deol, and M. S. P. Sansom. 2003. Lipid-protein interactions and the membrane/water interfacial region. *J. Am. Chem. Soc.* 125:14966–14967.

18. Gumbart, J., Y. Wang, A. Aksimentiev, E. Tajkhorshid, and K. Schulten. 2005. Molecular dynamics simulations of proteins in lipid bilayers. *Curr. Opin. Struct. Biol.* 15:423–431.

19. Bond, P. J., and M. S. P. Sansom. 2003. Membrane protein dynamics vs. environment: simulations of OmpA in a micelle and in a bilayer. *J. Mol. Biol.* 329:1035–1053.

20. Patargias, G., P. J. Bond, S. D. Deol, and M. S. P. Sansom. 2005. Molecular dynamics simulations of GlpF in a micelle vs. in a bilayer: conformational dynamics of a membrane protein as a function of environment. *J. Phys. Chem. B.* 109:575–582.

21. Braun, R., D. M. Engelman, and K. Schulten. 2004. Molecular dynamics simulations of micelle formation around dimeric Glycophorin A transmembrane helices. *Biophys. J.* 87:754–763.

22. Bond, P. J., J. M. Cuthbertson, S. D. Deol, and M. S. P. Sansom. 2004. MD simulations of spontaneous membrane protein/detergent micelle formation. *J. Am. Chem. Soc.* 126:15948–15949.

23. Booth, P. J., and A. R. Curran. 1999. Membrane protein folding. *Curr. Opin. Struct. Biol.* 9:115–121.

24. Brünger, A. T. 2001. Structure of proteins involved in synaptic vesicle fusion in neurons. *Annu. Rev. Biophys. Biomol. Struct.* 30:157–171.

25. Leontiadou, H., A. E. Mark, and S. J. Marrink. 2006. Antimicrobial peptides in action. *J. Am. Chem. Soc.* 128:12156–12161.

26. Marrink, S. J., A. H. de Vries, and A. E. Mark. 2004. Coarse grained model for semiquantitative lipid simulations. *J. Phys. Chem. B.* 108:750–760.

27. Murtola, T., E. Falck, M. Patra, M. Karttunen, and I. Vattulainen. 2004. Coarse-grained model for phospholipid/cholesterol bilayer. *J. Chem. Phys.* 121:9156–9165.

28. Nielsen, S. O., C. F. Lopez, G. Srinivas, and M. L. Klein. 2004. Coarse grain models and the computer simulation of soft materials. *J. Phys. Condens. Matter.* 16:R481–R512.

29. Stevens, M. J. 2004. Coarse-grained simulations of lipid bilayers. *J. Chem. Phys.* 121:11942–11948.

30. Tozzini, V. 2005. Coarse-grained models for proteins. *Curr. Opin. Struct. Biol.* 15:144–150.

31. Izvekov, S., and G. A. Voth. 2005. A multiscale coarse-graining method for biomolecular systems. *J. Phys. Chem. B.* 109:2469–2473.

32. Shi, Q., S. Izvekov, and G. A. Voth. 2006. Mixed atomistic and coarse-grained molecular dynamics: simulation of a membrane bound ion channel. *J. Phys. Chem. B.* 110:15045–15048.

33. Shih, A. Y., A. Arkhipov, P. L. Freddolino, and K. Schulten. 2006. Coarse grained protein-lipid model with application to lipoprotein particles. *J. Phys. Chem. B.* 110:3674–3684.

34. Han, W., and Y. D. Wu. 2007. Coarse-grained protein model coupled with a coarse-grained water model: molecular dynamics study of polyalanine-based peptides. *J. Chem. Theory Comput.* 3:2146–2161.

35. Shelley, J. C., M. Y. Shelley, R. C. Reeder, S. Bandyopadhyay, and M. L. Klein. 2001. A coarse grain model for phospholipid simulations. *J. Phys. Chem. B.* 105:4464–4470.

36. Nielsen, S. O., C. F. Lopez, I. Ivanov, P. B. Moore, J. C. Shelley, and M. L. Klein. 2004. Transmembrane peptide-induced lipid sorting and mechanism of L- alpha-to-inverted phase transition using coarse-grain molecular dynamics. *Biophys. J.* 87:2107–2115.

37. Venturoli, M., B. Smit, and M. M. Sperotto. 2005. Simulation studies of protein-induced bilayer deformations, and lipid-induced protein tilting, on a mesoscopic model for lipid bilayers with embedded proteins. *Biophys. J.* 88:1778–1798.

38. Bond, P. J., and M. S. P. Sansom. 2006. Insertion and assembly of membrane proteins via simulation. *J. Am. Chem. Soc.* 128:2697–2704.

39. Bond, P. J., and M. S. P. Sansom. 2007. Bilayer deformation by the Kv channel voltage sensor domain revealed by self-assembly simulations. *Proc. Natl. Acad. Sci. USA.* 104:2631–2636.

40. Sansom, M. S. P., K. A. Scott, and P. J. Bond. 2008. Coarse grained simulation: a high throughput computational approach to membrane proteins. *Biochem. Soc. Trans.* 36:27–32.

41. Bond, P. J., J. Holyoake, A. Ivetac, S. Khalid, and M. S. P. Sansom. 2007. Coarse-grained molecular dynamics simulations of membrane proteins and peptides. *J. Struct. Biol.* 157:593–605.

42. Periole, X., T. Huber, S. J. Marrink, and T. P. Sakmar. 2007. G protein-coupled receptors self-assemble in dynamics simulations of model bilayers. *J. Am. Chem. Soc.* 129:10126–10132.

43. Killian, J. A., and G. von Heijne. 2000. How proteins adapt to a membrane-water interface. *Trends Biochem. Sci.* 25:429–434.

44. Killian, J. A., and T. K. M. Nyholm. 2006. Peptides in lipid bilayers: the power of simple models. *Curr. Opin. Struct. Biol.* 16:473–479.

45. Berendsen, H. J. C., D. van der Spoel, and R. van Drunen. 1995. GROMACS: a message-passing parallel molecular dynamics implementation. *Comput. Phys. Commun.* 95:43–56.

46. Lindahl, E., B. Hess, and D. van der Spoel. 2001. GROMACS 3.0: a package for molecular simulation and trajectory analysis. *J. Mol. Model.* 7:306–317.

47. Bond, P. J., J. P. Derrick, and M. S. P. Sansom. 2007. Membrane simulations of OpcA: gating in the loops? *Biophys. J.* 92:L23–L25.

48. Berendsen, H. J. C., J. P. M. Postma, W. F. van Gunsteren, A. DiNola, and J. R. Haak. 1984. Molecular dynamics with coupling to an external bath. *J. Chem. Phys.* 81:3684–3690.

49. Humphrey, W., A. Dalke, and K. Schulten. 1996. VMD—visual molecular dynamics. *J. Mol. Graph.* 14:33–38.

50. Sayle, R. A., and E. J. Milner-White. 1995. RasMol: biomolecular graphics for all. *Trends Biochem. Sci.* 20:374–376.

51. Marrink, S. J., E. Lindahl, O. Edholm, and A. E. Mark. 2001. Simulation of the spontaneous aggregation of phospholipids into bilayers. *J. Am. Chem. Soc.* 123:8638–8639.

52. Monticelli, L., S. K. Kandasamy, X. Periole, R. G. Larson, D. P. Tieleman, and S. J. Marrink. 2008. The MARTINI coarse grained force field: extension to proteins. *J. Comput. Theor. Chem.* 4:819–834.

53. Sparr, E., W. L. Ash, P. V. Nazarov, D. T. S. Rijkers, M. A. Hemminga, D. P. Tieleman, and J. A. Killian. 2005. Self-association of transmembrane

alpha-helices in model membranes—importance of helix orientation and role of hydrophobic mismatch. *J. Biol. Chem.* 280:39324–39331.

54. Marrink, S. J., and A. E. Mark. 2003. Molecular dynamics simulation of the formation, structure, and dynamics of small phospholipid vesicles. *J. Am. Chem. Soc.* 125:15233–15242.

55. Sansom, M. S. P. 1993. Structure and function of channel-forming peptaibols. *Q. Rev. Biophys.* 26:365–421.

56. Lyubartsev, A. P. 2005. Multiscale modeling of lipids and lipid bilayers. *Eur. Biophys. J.* 35:53–61.

57. Chang, R., G. S. Ayton, and G. A. Voth. 2005. Multiscale coupling of mesoscopic- and atomistic-level lipid bilayer simulations. *J. Chem. Phys.* 122:244716.

58. Marrink, S. J., J. Risselada, S. Yefimov, D. P. Tieleman, and A. H. de Vries. 2007. The MARTINI forcefield: coarse grained model for biomolecular simulations. *J. Phys. Chem. B.* 111:7812–7824.

59. Cuthbertson, J. M., P. J. Bond, and M. S. P. Sansom. 2006. Transmembrane helix-helix interactions: comparative simulations of the glycophorin A dimer. *Biochemistry.* 45:14298–14310.

60. Halgren, T. A., and W. Damm. 2001. Polarizable force fields. *Curr. Opin. Struct. Biol.* 11:236–242.

61. Tieleman, D. P., H. Leontiadou, A. E. Mark, and S. J. Marrink. 2003. Simulation of pore formation in lipid bilayers by mechanical stress and electric fields. *J. Am. Chem. Soc.* 125:6382–6383.

62. Gurtovenko, A. A., and I. Vattulainen. 2005. Pore formation coupled to ion transport through lipid membranes as induced by transmembrane ionic charge imbalance: atomistic molecular dynamics study. *J. Am. Chem. Soc.* 127:17570–17571.

63. Reynwar, B. J., G. Illya, V. A. Harmandaris, M. M. Müller, K. Kremer, and M. Deserno. 2007. Aggregation and vesiculation of membrane proteins by curvature-mediated interactions. *Nature.* 447:461–464.